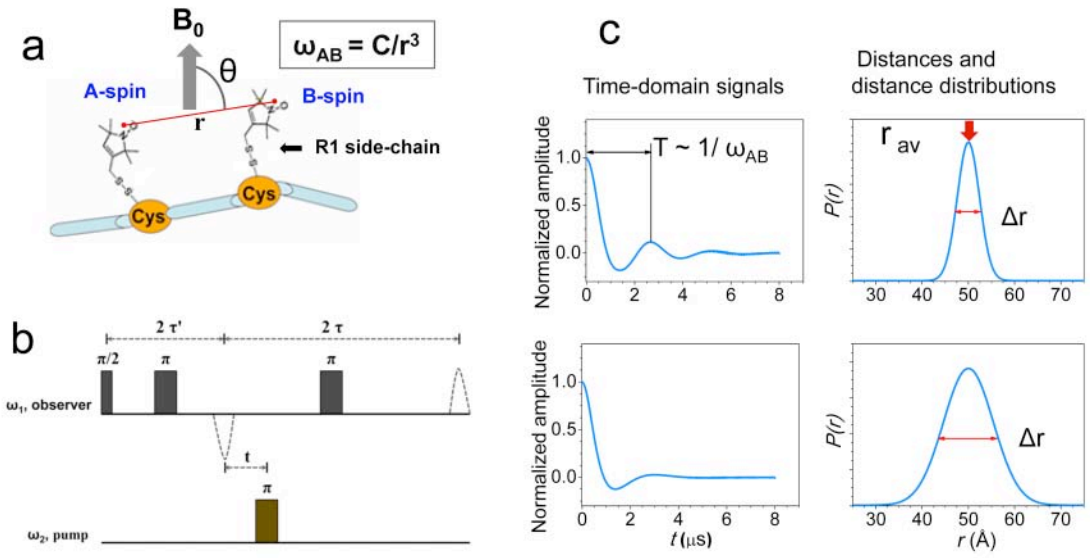


**Supplementary Figure 1. Four-pulse DEER method to measure distances between nitroxide spin-labels attached to cysteines.** (**a**) A cartoon of a doubly spin-labeled polypeptide chain, where $\mathbf{B}_0$ denotes external magnetic field, $\theta$ is the angle between $\mathbf{B}_0$ and the vector **r** connecting the NO groups; dipolar frequency $\omega_{AB} \propto 1/r^3$ is used to determine the distance $r$. The cysteine residue with attached nitroxide label is denoted as R1. (**b**) Pulse sequence used in DEER experiment. Three microwave pulses with fixed positions are applied to spins A at the "observer" frequency $\omega_1$ to form the echo. Variable-position 4-th "pump" pulse is applied between the last two observer pulses at frequency $\omega_2$ to flip spins B, thereby changing the sign of dipole-dipole interaction and the amplitude of the spin-echo. The result is the echo amplitude modulation as a function of pump pulse position, $t$. (**c**) Simulated echo modulations (left). These modulations were computed for the average distance $r_{av}$ of 50 Å and two Gaussian distributions in $r$ (right) with different widths $\Delta r$ (top and bottom). These distributions may originate from the conformational flexibility of R1 side chain and/or the protein molecule.

Nature Structural & Molecular Biology: doi:10.1038/nsmb.2494

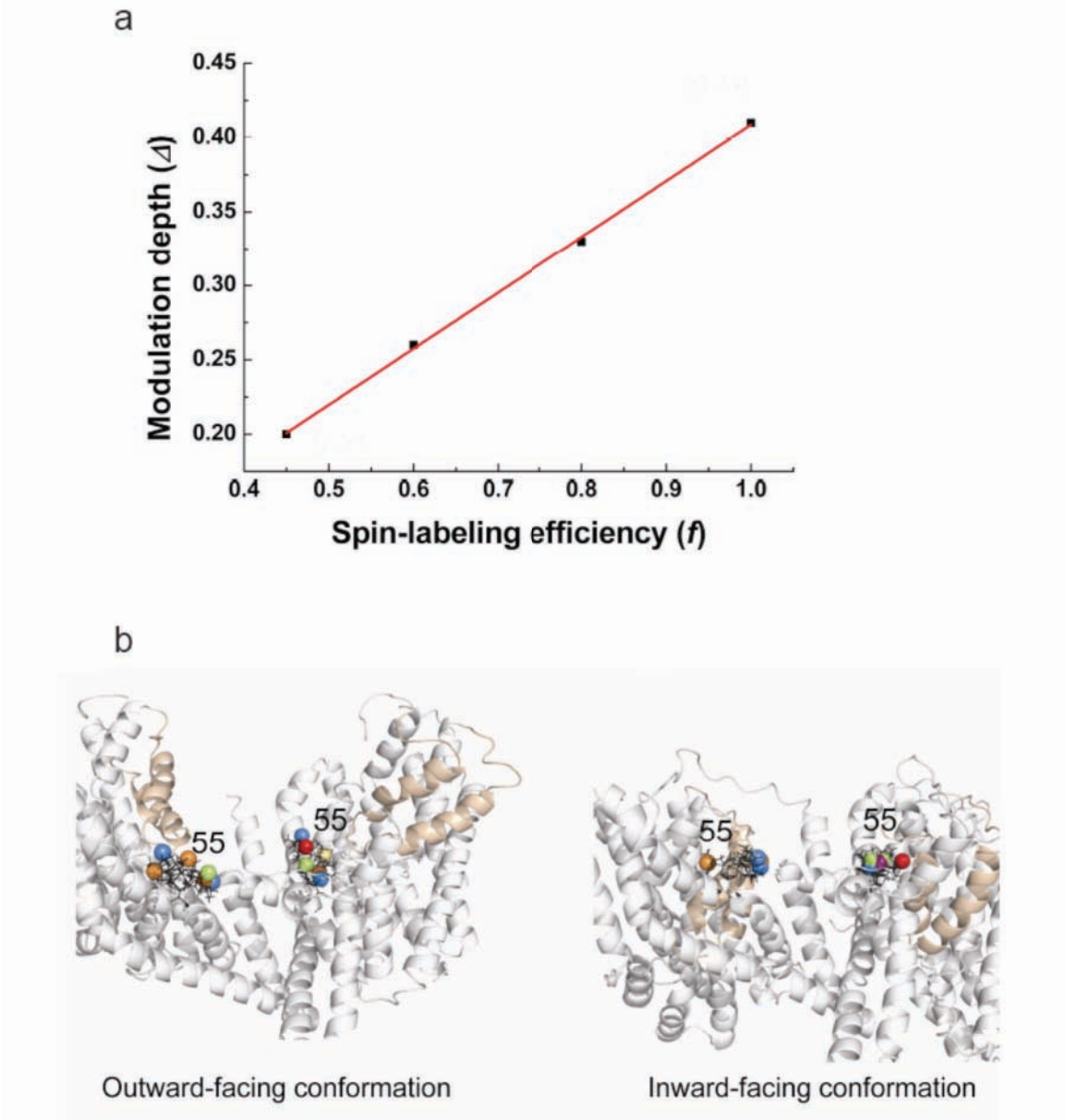


**Supplementary Figure 2. DEER data analysis.** (**a**) The dependence of the modulation depth, $\Delta$, of the time-domain DEER signal on spin-labeling efficiency for a three-spin system. The modulation depth was calculated using Eq. S4 for spin-labeling efficiency, $f$, varied from 0.45 to 1.0. (**b**) Modeling of R1 orientation using energy weighted rotamers. Two protomers of $Glt_{Ph}$ are shown in the outward (left panel) inward (right panel) facing conformation. The rotamers generated for residue 55R1 are rendered as sticks, with the oxygen atoms of the NO groups rendered as spheres. The sphere color-coding scheme is defined by rotamer population as follows: 50-40 %, purple; 30-21 %, red; 20-16 %, orange; 11-15 %, yellow; 6-10 %, green; 5 % or less in blue.

Nature Structural & Molecular Biology: doi:10.1038/nsmb.2494

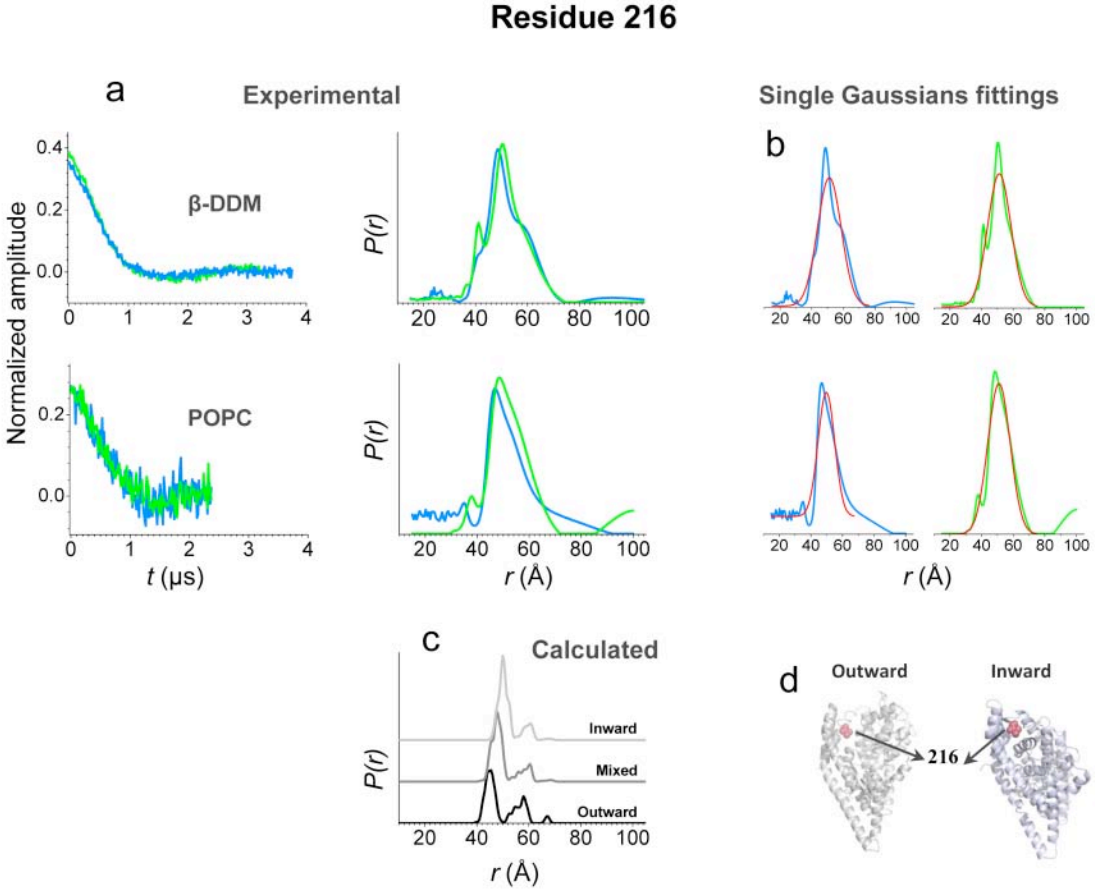


**Supplementary Figure 3. DEER analysis of the spin-labeled trimerization domain mutant V216R1.** (**a**) The experimental data for protein in detergent (upper panel) and lipid (lower panel): background-corrected normalized time-domain DEER data (left), and reconstructed distance distributions (right). The data for apo and substrate-bound protein are colored blue and green, respectively. (**b**) The fits of the experimental distance distributions in panel **a** to single Gaussians are shown in red together with the experimental distance distributions for protein in detergent (upper panel) and lipid (lower panel). The parameters of Gaussians are listed in Supplementary Table 1. (**c**) The distance distributions computed for rotamers with populations evaluated at 175 K for three configurations of $Glt_{Ph}$ subunit pairs: symmetric outward (bottom); mixed (middle); and symmetric inward (top). (**d**) A cartoon representation of a single $Glt_{Ph}$ protomer in the outward and inward facing states. Residue 216 is rendered as red spheres.

Nature Structural & Molecular Biology: doi:10.1038/nsmb.2494

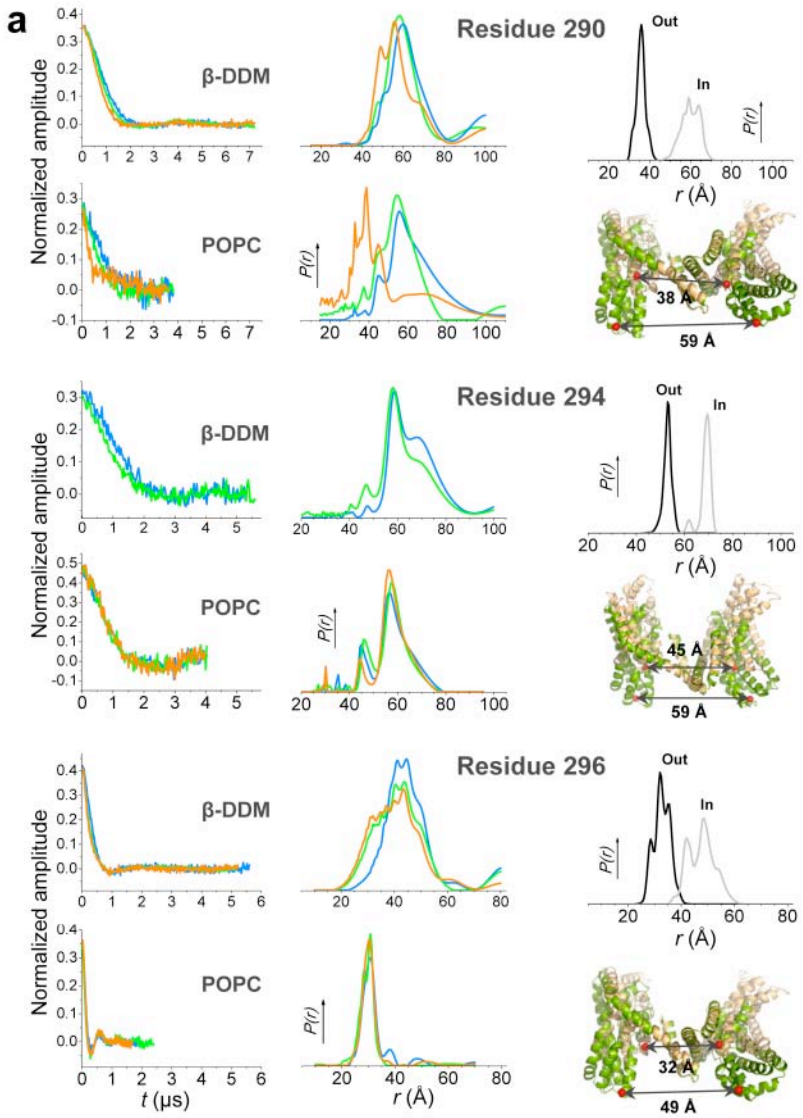


**Supplementary Figure 4 (continues)**

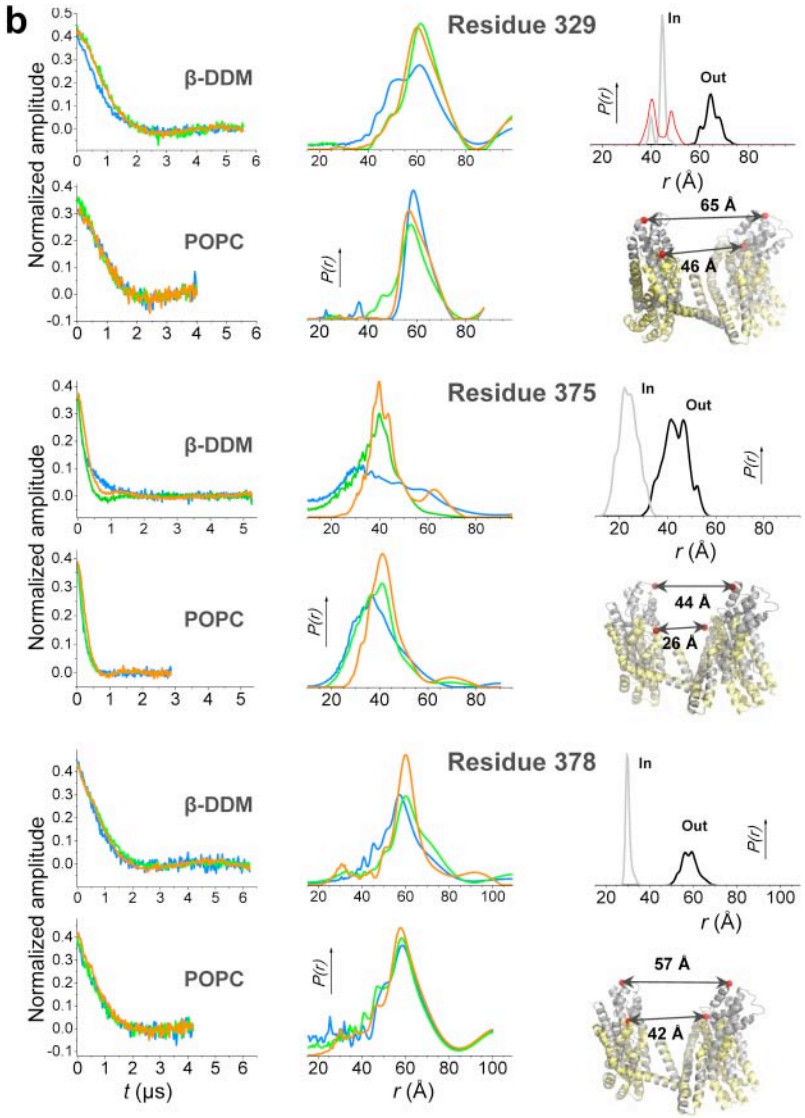


**Supplementary Figure 4 (continues)**

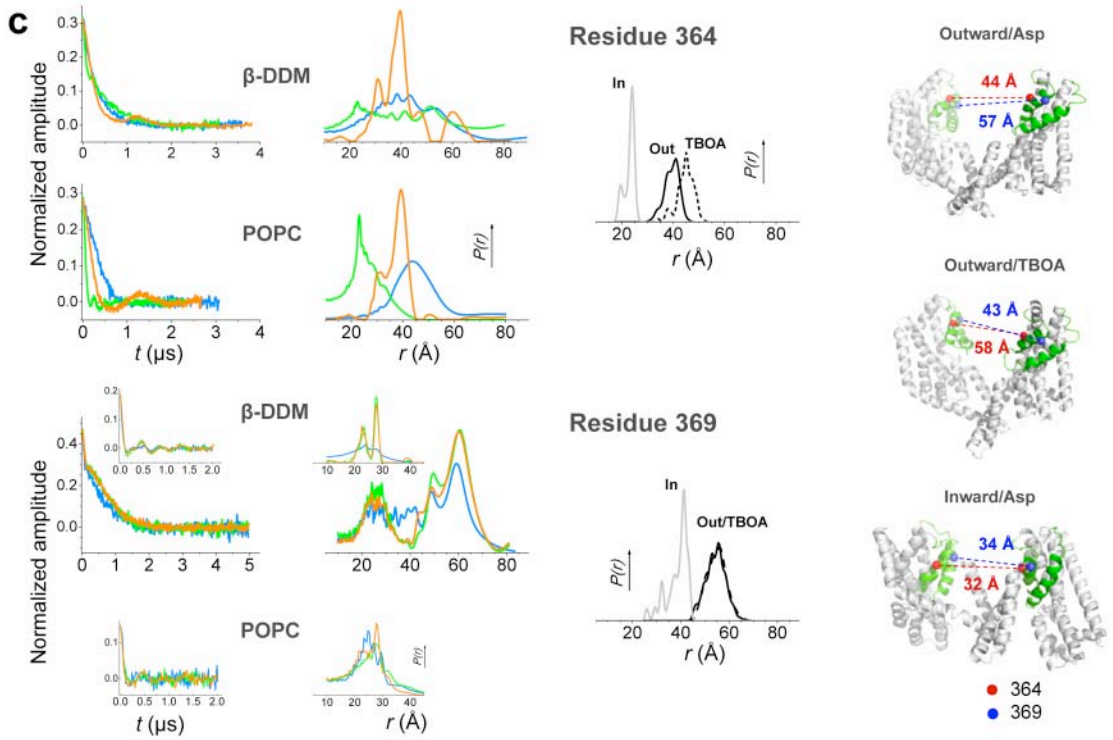


**Supplementary Figure 4. DEER analysis of the spin-labeled transport domain mutants.** (**a**) Intracellular K290R1, I294R1 and E296R1. **(b**) Extracellular L329R1, T375R1 and N378R1. (**c**) HP2 mutants A364R1 and S369R1. Experimental background-corrected and normalized DEER time-domain data (leftmost) together with the reconstructed distance distributions (center) in detergent and lipid, as indicated. Data for the apo Asp- and TBOA-bound transporters are in blue, green and orange, respectively. The short-distance component of the DEER signals for 369R1 plotted for 2 μs evolution time is shown in the inset of panel **c**. In this case, the signal from the long distance component was treated as background, approximated by a polynomial and subtracted out. For this residue, we were unable to record DEER signals for evolution times exceeding 2 μs in lipid bilayers, limited by the fast phase relaxation. The distance distributions (right) computed using rotamer libraries are plotted for the symmetric outward (black) and inward (gray) facing configurations alongside with the superimposed structures of two $Glt_{Ph}$ protomers in the outward (tan or gray in **a** and **b**, respectively) and inward (green or yellow in **a** and **b**, respectively) facing states. The rotamer-based computed distances for residues 364R1 and 369R1 in panel **c** are shown in the middle column between experimental data and structures (in gray with HP2 colored green) of two $Glt_{Ph}$ protomers in outward facing conformation either with Asp or TBOA, and inward facing conformation. In all structures shown, the residues 10-150 are removed for clarity. The $C_\beta$ atoms of labeled residues are shown as colored spheres, and the $C_\beta$-$C_\beta$ distances are indicated.

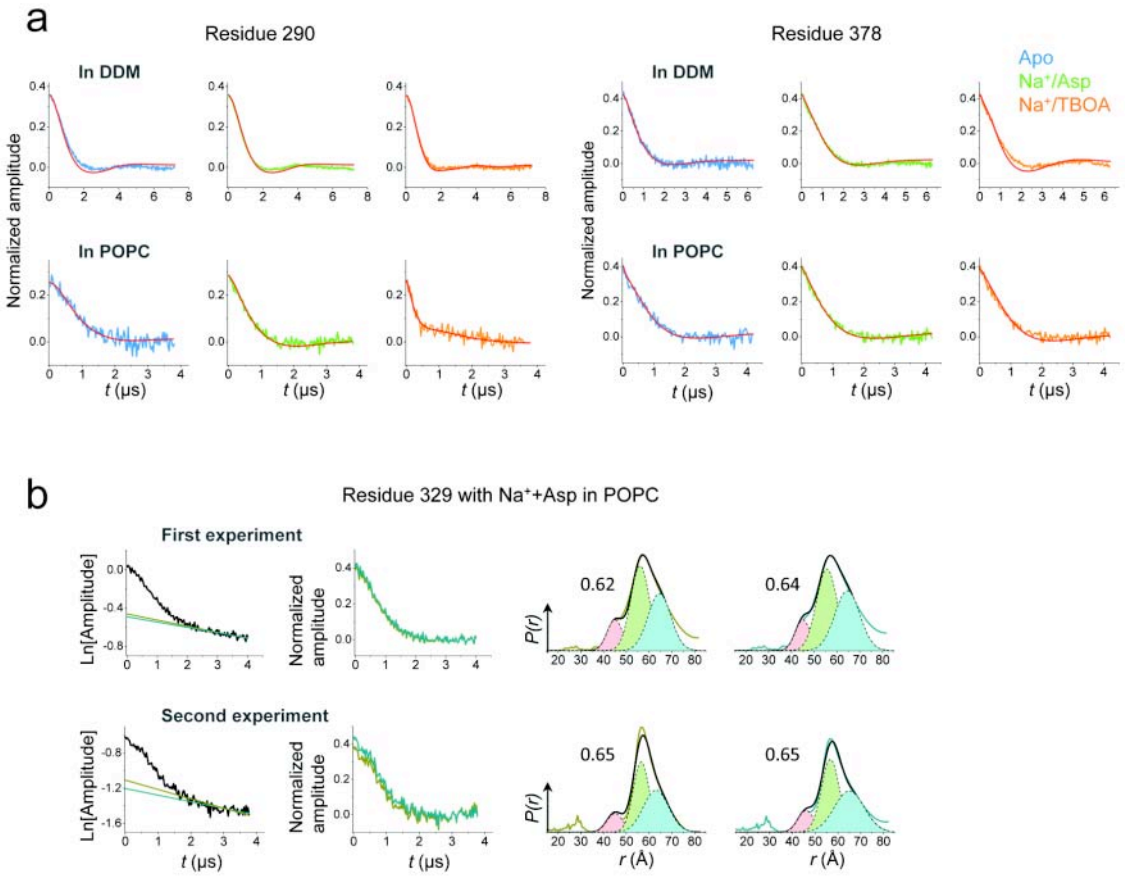


**Supplementary Figure 5. Robustness and reliability of the distance distributions analysis.** (**a**) Correspondence between the experimental time-domain DEER data (blue, green and orange for apo, Asp- and TBOA-bound $Glt_{Ph}$, respectively) and the time-domain signals generated from the three-Gaussian fits (red). The data for labeled residues 290 and 378 (left and right panels, respectively) are shown. (**b**) The effect of base-line subtraction on the distances and distance distributions. DEER data were collected for residue 329R1 in lipid and in the presence of $Na^+$ and Asp in two independent experiments. The raw time-domain data on semi-logarithmic scale is in the leftmost column. Data are black and two baselines are in shades of green. A homogeneous 3D background signal was used. The baseline variations mainly affect the amplitude of the normalized dipolar signals that differ in the modulation depth as shown in the second column (colors correspond to those of the baselines in the leftmost panels). The reconstructed distance distributions from each of the signals in the second panels were analyzed by fitting them to three Gaussians, and the results for the first and second experiments are shown in the third and fourth columns, respectively. The experimental distance distributions are in colors, corresponding to the baselines in the first data column. The envelopes of three-Gaussian fits are in black with individual Gaussians color-coded as in Figure 3. The fitting parameters are in Supplementary Table 3.

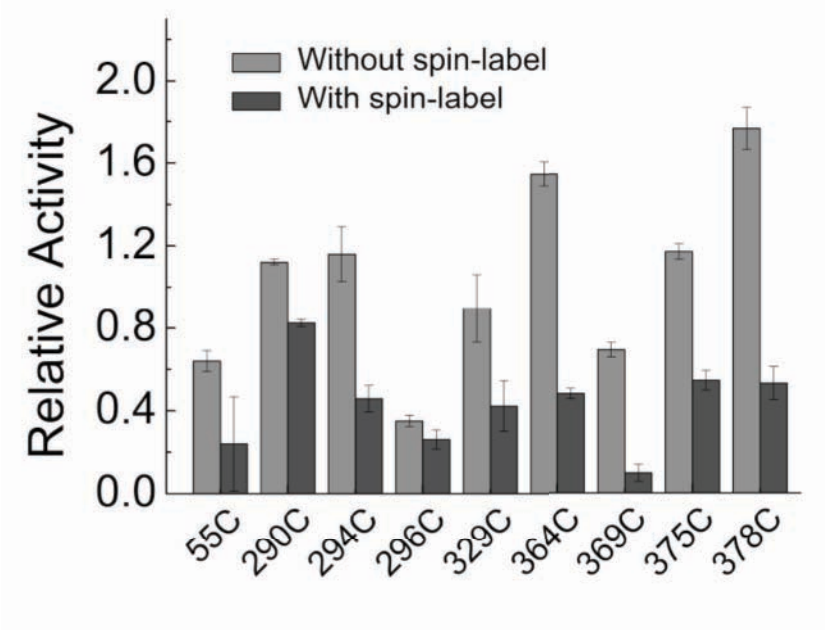


**Supplementary Figure 6. Aspartate uptake by spin-labeled mutants.** Wild type cysteine-less $Glt_{Ph}$ and single cysteine mutants before and after spin-labeleing were reconstituted into POPC liposomes and assayed for $Na^+$ driven concentrative aspartate transport. Background uptake was determined in the absence of $Na^+$ gradient and subtracted from the data. Activities relative to the wild type are shown. The data represent the mean and standard deviation of three experiments for each cysteine mutant and six experiments for the wild type protein.

**Supplementary Table 1. The predicted and measured distances**

| Residue | | $C_\beta$-$C_\beta$[$] (rotamers) | Measured distances[#] | | | | | |
|---|---|---|---|---|---|---|---|---|
| | | | *DDM** | | | *POPC* | | |
| | | | *Apo* | *Asp* | *TBOA* | *Apo* | *Asp* | *TBOA* |
| 55 | | 28 (27) | 25 ± 1.7 | 28 ± 1.4 | 24 ± 2.3 | 23 ± 2.2 | 22 ± 2.2 | 25 ± 2.1 |
| 216 | | 56 (51) | 51 ± 3.8 | 51 ± 3.7 | N/A | 50 ± 2.6 | 51 ± 3.5 | N/A |
| 290 | out | 38 (36) | 48 ± 1.8 | 49 ± 1.7 | 48 ± 1.4 | 43 ± 2.0 | 42 ± 2.3 | 38 ± 2.3 |
| | mix | 52 (51) | 57 ± 2.1 | 58 ± 2.1 | 56 ± 1.9 | 55 ± 2.5 | 54 ± 2.5 | 63 ± 3.3 |
| | in | 59 (60) | 63 ± 2.9 | 66 ± 2.9 | 68 ± 2.5 | 67 ± 4.5 | 63 ± 3.3 | 70 ± 3.5 |
| 294 | out | 45 (53) | 46 ± 1.5 | 46 ± 1.5 | N/A | 46 ± 1.3 | 47 ± 1.1 | 45 ± 1.0 |
| | mix | 55 (62) | 59 ± 1.7 | 58 ± 1.7 | N/A | 60 ± 1.5 | 57 ± 1.4 | 56 ± 1.3 |
| | in | 59 (69) | 69 ± 3.5 | 69 ± 3.5 | N/A | 66 ± 2.3 | 64 ± 2.3 | 63 ± 2.5 |
| 296 | out | 32 (33) | 35 ± 1.7 | 32 ± 1.9 | 32 ± 2.3 | 30 ± 1.2 | 30 ± 1.2 | 30 ± 1.1 |
| | mix | 45 (44) | 42 ± 1.9 | 42 ± 1.9 | 42 ± 2.4 | -[&] | - | - |
| | in | 49 (48) | 49 ± 2.0 | 51 ± 1.9 | 51 ± 2.5 | - | - | - |
| 329 | out | 65 (65) | 70 ± 2.8 | 68 ± 2.5 | 67 ± 2.5 | 63 ± 2.5 | 63 ± 2.5 | 61 ± 2.5 |
| | mix | 57 (56) | 60 ± 2.7 | 60 ± 2.0 | 59 ± 2.0 | 57 ± 1.6 | 56 ± 1.9 | 56 ± 1.9 |
| | in | 46 (44) | 49 ± 2.4 | 50 ± 1.9 | 48 ± 1.9 | 36 ± 1.5 | 45 ± 1.8 | 38 ± 1.8 |
| 375 | out | 44 (43) | 59 ± 4.8 | 45 ± 2.5 | 45 ± 2.8 | 51 ± 2.7 | 45 ± 3.4 | 46 ± 2.7 |
| | mix | 40 (39) | 51 ± 4.3 | 38 ± 2.1 | 39 ± 1.8 | 39 ± 2.7 | 39 ± 2.9 | 40 ± 1.9 |
| | in | 26 (24) | 31 ± 3.8 | 25 ± 3.4 | 31 ± 1.5 | 30 ± 2.5 | 31 ± 2.7 | 33 ± 1.7 |
| 378 | out | 57 (58) | 65 ± 4.5 | 67 ± 4.3 | 62 ± 2.4 | 62 ± 3.0 | 61 ± 3.1 | 64 ± 3.5 |
| | mix | 52 (47) | 56 ± 2.9 | 59 ± 2.9 | 57 ± 2.4 | 53 ± 2.9 | 50 ± 4.2 | 55 ± 3.3 |
| | in | 42 (30) | 43 ± 2.5 | 36 ± 2.3 | 32 ± 2.5 | 28 ± 2.8 | 35 ± 5.0 | 35 ± 3.0 |
| 364 | out | 44 (39) | 54 ± 3.0 | 52 ± 2.3 | 40 ± 1.6 | 48 ± 3.0 | 40 ± 1.7 | 39 ± 1.3 |
| | mix | 42 (35) | 40 ± 3.4 | 35 ± 4.0 | 31 ± 1.4 | 41 ± 2.3 | 31 ± 1.6 | 31 ± 1.3 |
| | in | 32 (23) | 27 ± 3.6 | 23 ± 1.5 | 23 ± 1.1 | 30 ± 1.9 | 23 ± 1.4 | 20 ± 1.4 |
| 369 | out | 57 (54) | 61 ± 1.5 | 62 ± 1.6 | 62 ± 1.7 | N/A | N/A | N/A |
| | mix | 49 (50) | 49 ± 3.8 | 55 ± 3.0 | 54 ± 3.5 | N/A | N/A | N/A |
| | in | 34 (39) | 26 ± 4.0 | 26 ± 2.8 | 25 ± 3.0 | N/A | N/A | N/A |

[$] Average distances based on the crystal structures of the outward and inward facing states of $Glt_{Ph}$, (pdb: 2NWX, 3KBC, respectively). Calculated average distances based on the rotamer libraries with populations estimated at 175 K are shown in the brackets. All distances are given in angstroms. [#] Distances obtained from fitting experimental distance distributions to single Gaussians. Shown are Gaussian means ±0.5 of the standard deviations. * The measurements were performed using protein samples in DDM or POPC under the following ligand conditions. Apo: no sodium or Asp; Asp: 100 mM NaCl and 100 µM Asp; TBOA: 50 mM NaCl and 125 µM TBOA. [&] Inward-facing state is not populated.

**Supplementary Table 2. The effect of baseline subtraction on the distance distributions for labeled residue 329 in POPC lipid.**

| State | Measured distances[#] | | | |
|---|---|---|---|---|
| | First Experiment | | Second Experiment | |
| | **A** | **B** | **A** | **B** |
| out | 64.5 ± 2.5 | 64.5 ± 2.75 | 63 ± 2.25 | 65 ± 3.25 |
| mix | 56 ± 2.0 | 56 ± 2.25 | 57 ± 1.75 | 57 ± 2.0 |
| in | 45 ± 1.7 | 45 ± 1.7 | 45 ± 1.75 | 46 ± 2.25 |

[#] Distances obtained from fitting experimental distance distributions to three Gaussians are listed. All distances are in Å. Data were collected from samples supplemented with 100 mM NaCl and 100 μ M Asp. * The numbers listed in the table correspond to the Gaussians plotted in Supplementary Figure 5a: **A** and **B** correspond to the third and fourth columns of the Figure, respectively. The means and widths of the individual calculated Gaussians were adjusted to achieve the best fits. Note that the variations in the values are small and they are also close to those obtained for the 329R1 data shown in Figure 3 (Supplementary Table 2). The differences in the Gaussians means and widths originate from varied baselines subtracted prior the distances reconstruction.

**Supplementary Note**

***Dipolar ESR spectroscopy.*** In this work all distance measurements were carried out using four-pulse double electron-electron resonance (DEER). [3-7] The method is based on measuring the strength of the static magnetic dipole-dipole interaction between unpaired electron spins, which is inversely proportional to the cube of distance between them. [8] The electron spins are usually those of nitroxide spin-labels covalently attached to cysteine residues within a single polypeptide chain or in a protein complex (Supplementary Figure 1a). For two electron spins this interaction, expressed in frequency units, is given by:

$$\omega_{\mathbf{r}} = \omega_0(r)(1 - 3\cos^2\theta), \qquad \text{(S1)}$$

where $\omega_0 = \gamma_e^2\hbar/r^3$ is called the dipolar frequency, $\gamma_e$ is the electron spin gyromagnetic ratio; $\hbar$ is Planck's constant divided by $2\pi$; $r=|\mathbf{r}|$ is the distance between the spins, in this case between the NO groups of the spin labels; $\theta$ is the angle between the direction of the external magnetic field $\mathbf{B}_0$ and the vector $\mathbf{r}$ connecting the NO groups.

In the 4-pulse DEER method (Supplementary Figure 1b), one detects the amplitude of the refocused primary echo, produced with the selective three-pulse sequence $\pi/2–\tau'–\pi–\tau'+\tau–\pi–\tau–$ *echo* applied at the "observer" frequency $\omega_1$. The spins, giving rise to the echo, are referred to as "A-spins", while the rest that do not contribute are referred to as "B-spins". An additional selective "pump" pulse, applied at frequency $\omega_2$, does not act on A-spins, but instead flips a fraction $p$ of B-spins, ($p$ is often denoted as $\lambda$ in the literature). This reverses the sign of the dipolar coupling between A- and B-spins, changing the precession frequency of the A spins by $\Delta\omega = \pm\omega_{\mathbf{r}}/2$. The detection sequence is fixed, while the position of the pump pulse, $t$, is advanced from the second to the third detection pulse. This produces modulation of the echo amplitude due to linear phase $2\Delta\omega t$, which is not refocused by the detection pulse sequence. The modulated signal, $V(t)$ is well described by [4,7]

$$V(t)/V_0 = (1 - p) + p\cos(\omega_{\mathbf{r}} t), \qquad \text{(S2)}$$



Nature Structural & Molecular Biology: doi:10.1038/nsmb.2494

where $V_0$ is the echo amplitude in the absence of the pump pulse. The second term in Eq. S2, oscillating with frequency $\omega_{\mathbf{r}}$, is referred to as the "dipolar signal". In isotropic samples, spins from molecules in all orientations contribute to the signal. This dipolar signal is described by an average over $\theta$, so it depends only on $r$ and decays to zero with $t$ due to the dephasing of the component signals with different values of $\cos(\theta)$, leaving a constant offset, $1 - p$. The decrease in the amplitude of the echo due to the pump pulse is referred to as the "modulation depth" and is equal to the amplitude of the second term of Eq. S2, the dipolar signal. Therefore, we use these terms interchangeably. Note that the period of oscillations is proportional to the cube of the distance between coupled electron spins (Supplementary Figure 1c). This is the main limitation to the distance that can be measured, since the echo amplitude diminishes with increased pulse separation due to several relaxation mechanisms [4]. Eq. S2 holds for an isolated pair of spins. In real samples, electron spins on surrounding molecules cause the decay of the echo amplitude with $t$, rendering the first term in Eq. S2 a decaying "baseline", which should be removed to leave the pure dipolar signal.

***The spin-labeling efficiency and multi-spin systems.*** Since $Glt_{Ph}$ is a trimer and can contain three spins, we comment on the additional specifics of a three-spin system. Data interpretation for biomolecules bearing more than two electron spins has been recently addressed in the literature [9,10], elaborating on an earlier work of Milov *et al* [11]. The effects of interactions between multiple spins were described in the context of spin-counting, establishing that for $N$ coupled spins the modulation depth, $\Delta$, of the time-domain DEER signal increases with the number of coupled spins as

$$\Delta(p) = 1 - (1 - p)^{N-1} \qquad \text{(S3)}$$

The modulation depth is thus different from that in a pair of spins, where it is just $p$. In our Ku-band (17.3 GHz) spectrometer $p$ usually is between 0.15 and 0.35 for $^{14}N$ nitroxides. However, if protein spin-labeling is incomplete, the number of interacting spins is also a function of the labeling efficiency, $f$, and the modulation depth becomes: [12]

$$\Delta(p, f) = 1 - (1 - fp)^{N-1} \qquad \text{(S4)}$$

That is $p$ is simply modified by $f$. It would seem beneficial from Eq. S2 to use a stronger pump pulse to increase the dipolar signal. However, based on the discussion below, we



Nature Structural & Molecular Biology: doi:10.1038/nsmb.2494

use in our experiments a detection pulse sequence with pulse widths of 16 ns – 32 ns – 32 ns and a pump $\pi$-pulse of 32 ns, corresponding to the amplitude of the rotating frame magnetic component of the microwave field [8] of the pump pulse, $B_1$, of 5.6 G. Such a pump pulse applied at the center of the 17.3 GHz nitroxide ESR spectrum has a $p$ of ~0.23, according to calculations and experimental measurements. However, for three spins one observes modulation, which is nearly twice this value. For a 100% labeled protein, the modulation depth according to Eq. S4 is 0.41. Using $p$ of 0.23 and spin-labeling efficiencies between 0.45 and 1, we calculated the DEER modulation depths expected for a three-spin system (Supplementary Figure 2a). The modulation depths obtained in our experiments (Supplementary Figures 3 and 4) are in the range between ~0.28 and 0.4, suggesting that the spin-labeling efficiency for all $Glt_{Ph}$ mutants was greater than ~65%.

***The three-spin system in $Glt_{Ph}$ mutants.*** The theoretical background and practical implications of the three-spin system in DEER spectroscopy is described in two recent studies by Jeschke *et al.* [12] and Bhatnagar *et al.* [9]. To simplify the discussion, we consider a protein with three potential labeling sites A, B and C. Only molecules bearing a spin at $\omega_1$ contribute to the echo. If this is spin A, the probability that one of sites B or C is both labeled and its spin flipped by the pump pulse is $p_f \equiv fp$. The probability that both or neither of the sites are labeled and their spins are flipped is $(p_f)^2$ and $(1 - p_f)^2$, respectively. Hence, the part of the experimental signal contributed by site A will contain [9,12] the following terms:

$$(1-p_f)^2 + p_f(\cos(\omega_{AB}t) + \cos(\omega_{AC}t)) + p_f^2 \cos(\omega_{AB}t)\cos(\omega_{AC}t). \quad \text{(S5)}$$

Here, $\omega_{AB}$, $\omega_{BC}$, and $\omega_{AC}$ are the respective dipolar coupling frequencies. The last term produces both sum and difference frequencies: $\omega_+ = \omega_{AB} + \omega_{AC}$ and $\omega_- = \omega_{AB} - \omega_{AC}$. It is clear that the contribution of this term to the overall signal will diminish for smaller $p_f$ at lower labeling and flipping efficiencies. The combination frequencies result in unwanted peaks at shorter and longer distances in the distance distributions, if reconstructed using standard methods [1] that do not consider such non-linear effects.



Nature Structural & Molecular Biology: doi:10.1038/nsmb.2494

We examined the importance of such effects for this work because most of $Glt_{Ph}$ cysteine mutants were efficiently spin-labeled. We followed the approach described by Jeschke *et al* [12] and applied it to the detergent-reconstituted substrate-bound $Glt_{Ph}$-K55C. The labeling site, positioned within the highly symmetrical trimerization domain, produces a narrow distance distribution and the labeling efficiency was close to unity. Therefore, the sum component should also be narrow and clearly visible. To develop this component, we varied the power of the pump pulse and hence the flipping efficiency $p$. The standard pulse sequence $\pi/2 - \pi - \pi$ (16 ns – 32 ns – 32 ns) was used for detection. The length of the pump pulse was constant at 14 ns, while the flipping angle varied between $\pi$ and $\pi/2\sqrt{2}$, corresponding to $B_1$ of 13 G and 4.6 G, respectively (Figure 2d). We observed that for all values of $B_1$ the main peak in the distance distribution has a maximum at ~28 Å, corresponding to the dipolar frequency of 2.37 MHz. The sum frequency $\omega_+$ at 4.74 MHz should yield an extra peak at ~22 Å. Indeed, we see a narrow feature at this position, which diminishes with the decreasing $B_1$, as expected. Importantly, when $B_1$ is less than 9.2 G, only a very small signal remains, indicating that at this lower $B_1$ the contribution from the three-spin coupling can be ignored. In all of our experiments, we thus used 32 ns (5.6 G) pump pulse, rendering the three-spin artifacts insignificant.

***DEER data analysis.*** The distance distributions were reconstructed from the dipolar signals by applying Tikhonov regularization method [1] and refined by the maximum entropy method (MEM) [2]. These procedures have been performed using in-house programs available for download (www.acert.cornell.edu). We note that simulating time domain data from distance distributions is straightforward, but the inverse problem of reconstructing distance distributions from the time domain data is much more challenging, for it is an ill-posed mathematical problem [1]. There are several approaches to obtain a class of physically meaningful solutions, of which Tikhonov regularization is a very efficient tool. It limits the range of solutions by enforcing their smooth behavior [1,13]. To determine the optimal regularization parameters, we employed the L-curve method [1]. This method is very efficient and for undistorted low-noise signals recorded over sufficient time it reconstructs the distributions preserving many details. However, the



Nature Structural & Molecular Biology: doi:10.1038/nsmb.2494

solutions for distance distributions are not constrained to be positive for all values of *r*; therefore the distributions are usually refined by MEM to address this issue. MEM also allows one to increase the resolution at the expense of making the solutions somewhat less constrained.

Prior to the extraction of the distance information from pure dipolar signal, it should be isolated from the raw time domain data as previously described [14]. Briefly, the constant term in the DEER signal is modified by inter-molecular spin-spin interactions, [4,5,7], which usually contribute a decaying baseline well approximated by a single exponential decay. To remove the baseline, the logarithm of the data is fit to a straight line using the later points; the fit is extrapolated to zero time and subtracted out. Sometimes, a low-order polynomial is used in the fits, such as is the case of liposomes, where the decay is described by stretched exponentials [4]. The remaining signal $V(t)$ is brought back to a linear scale and processed as $(V(t) - 1)/V(0)$, to give the value of the modulation depth at zero time. This gives the pure intra-molecular dipolar signal. In the current study for all cases, including $Glt_{Ph}$ in detergent and POPC, a three-dimensional baseline contributing to the original DEER time-domain signal was subtracted as a linear background on a semi-logarithmic scale, since for trans-membrane proteins in detergent and lipid multilamellar vesicles the microscopic arrangement of spin-labeled protein molecules it is highly homogeneous [5].

***Robustness and reliability of the distance distributions analysis***. The 'goodness' of all three-Gaussians fits was estimated from the statistical parameter 'Adjusted $R^2$', as introduced by the OriginLab manual. The values of this parameter ranged from 0.8 to 0.99, showing that three Gaussians described the distance distributions well. To further verify the reliability of our data analysis, we compared the experimental time domain data to the time domain data back-calculated from the three-Gaussian fits, using simple MATLAB (*MathWorks, Inc*) program (Supplementary Figure 5a). Our results show that the experimental time-domain data are well reproduced. We believe that the small differences between calculated and experimental DEER signals are due to the fact that



Nature Structural & Molecular Biology: doi:10.1038/nsmb.2494

the actual distance distributions are not precisely Gaussians and may have some long-distance "tails" originating from baseline uncertainty of broad distributions.

The effects of baseline subtraction on the distances and distance distributions were tested by subtracting homogeneous baselines with slopes, which were varied manually on a semi-logarithm scale, prior to reconstructing distance distributions. Almost all of our raw DEER data had sufficiently high signal to noise ratios and evolution times, which did not provide a large room for variations in the baseline. These variations had only minor effects on the Gaussian means and widths obtained from the distance distributions analyses. Most importantly, the fittings of distance distributions show that populations of the outward and inward facing states are the least sensitive to the baseline variations. This is demonstrated in Supplementary Figure 5b and Supplementary Table 2 for residue 329R in lipid environment and in the presence of substrate. For a total of five different baselines (including the results shown in Figure 3b) and dipolar signals from two different experiments, we obtained an averaged population of the outward facing state $p_O$ = 0.64 ± 3% standard error. This outcome is expected, since the weights of components are represented by their relative contributions to amplitudes of the dipolar signal at zero time. This would not be very sensitive to reasonable baseline variations. It could affect the widths of the components, but areas are less sensitive.

***Accessible range of distances***. In general, the range of accessible distances in DEER is defined by the longest dipolar evolution time that can be used to obtain a signal with sufficient S/N and the upper limit could be set by [15]**:**

$$r_{\max} = 5\sqrt[3]{t_{\max}/(2\mu s)} \text{ in nm} \qquad \text{(S5)}$$

In most cases, we used dipolar evolution times longer than 4 μs and as much as 7 μs. As expected, the phase memory relaxation times (T2s) in lipid-reconstituted protein were shorter than those in detergent and set an upper limit for the evolution times of about 4 μs. Nevertheless, according to (S5), DEER data recorded on a 4 μs time-scale are sufficient to extract accurate distances of up to 6.3 nm. Indeed, more than 95 % of our distances are well within this range (Supplementary Table 1). We should mention that the long-range part of the distribution might be affected by the baseline subtraction, but these



Nature Structural & Molecular Biology: doi:10.1038/nsmb.2494

effects are minor (Supplementary Figure 5b). Residue 216R1 in trimerization domain is an exception. The lipid-reconstituted protein was only at 10 μM trimer concentration and the dipolar evolution times of about 2.5 μs were used (Supplementary Figure 3). This evolution time is insufficient to extract unambiguous distributions up to 60 Å. However, the measured averaged distance of ~50 Å is within the accessible range. Furthermore, we did not use distance distributions for residue 216 in quantitative analysis.

## Supplementary references


1. Chiang, Y.W., Borbat, P.P. & Freed, J.H. The determination of pair distance distributions by pulsed ESR using Tikhonov regularization. *J Magn Reson* **172**, 279-95 (2005).

2. Chiang, Y.W., Borbat, P.P. & Freed, J.H. Maximum entropy: a complement to Tikhonov regularization for determination of pair distance distributions by pulsed ESR. *J Magn Reson* **177**, 184-96 (2005).

3. Pannier, M., Veit, S., Godt, A., Jeschke, G. & Spiess, H.W. Dead-time free measurement of dipole-dipole interactions between electron spins. 2000. *J Magn Reson* **213**, 316-25 (2011).

4. Jeschke, G. & Polyhach, Y. Distance measurements on spin-labelled biomacromolecules by pulsed electron paramagnetic resonance. *Phys Chem Chem Phys* **9**, 1895-910 (2007).

5. Borbat, P.P. & Freed, J.H. Measuring distances by pulsed dipolar ESR spectroscopy: spin-labeled histidine kinases. *Methods Enzymol* **423**, 52-116 (2007).

6. Schiemann, O. & Prisner, T.F. Long-range distance determinations in biomacromolecules by EPR spectroscopy. *Q Rev Biophys* **40**, 1-53 (2007).

7. Borbat, P.P. & Freed, J.H. Pros and Cons of Pulse Dipolar ESR: DQC and DEER. *EPR Newsletter* **17**, 21-33 (2007).

8. Abragam, A. Principles of Nuclear Magnetism. *Oxford University Press Inc.* (1961).

9. Bhatnagar, J. et al. Structure of the ternary complex formed by a chemotaxis receptor signaling domain, the CheA histidine kinase, and the coupling protein CheW as determined by pulsed dipolar ESR spectroscopy. *Biochemistry* **49**, 3824-41 (2010).

10. Bode, B.E. et al. Counting the monomers in nanometer-sized oligomers by pulsed electron-electron double resonance. *J Am Chem Soc* **129**, 6736-45 (2007).

11. Milov, A.D., Ponomarev, A.B. & Tsvetkov, Y.D. Modulation beats of signal of double electron-electron resonance in spin echo for biradical systems *Journal of Structural Chemistry* **25**, 710-713 (1984).




Nature Structural & Molecular Biology: doi:10.1038/nsmb.2494

12. Jeschke, G., Sajid, M., Schulte, M. & Godt, A. Three-spin correlations in double electron-electron resonance. *Phys Chem Chem Phys* **11**, 6580-91 (2009).

13. Jeschke, G., Koch, A., Jonas, U. & Godt, A. Direct conversion of EPR dipolar time evolution data to distance distributions. *J Magn Reson* **155**, 72-82 (2002).

14. Georgieva, E.R. et al. Effect of freezing conditions on distances and their distributions derived from Double Electron Electron Resonance (DEER): A study of doubly-spin-labeled T4 lysozyme. *J Magn Reson* **216**, 69-77 (2012).

15. Jeschke, G. DEER distance measurements on proteins. *Annu Rev Phys Chem* **63**, 419-46 (2012).



Nature Structural & Molecular Biology: doi:10.1038/nsmb.2494